DOI: 10.13009/EUCASS2023-978
Aerospace Europe Conference 2023 – 10TH EUCASS – 9TH CEAS

Multiphase and Multidimensional Effects on Solid Rocket Nozzle Performance

M. Grossi[⋆†], *G. Cocirla*[⋆], *A. Sereno, D. Bianchi*[⋆] *and B. Favini*[⋆]
[⋆]*Dept. of Mechanical and Aerospace Engineering - Sapienza University of Rome*
Via Eudossiana 18, 00184 - Rome, Italy
marco.grossi@uniroma1.it · alessio.sereno@uniroma1.it · gianluca.cocirla@uniroma1.it · daniele.bianchi@uniroma1.it · bernardo.favini@uniroma1.it
[†]Corresponding author

Abstract

This study investigates the influence of three-dimensional and two-phase contributions to the performance of aft-finocyl solid rocket motors. Single-phase and multiphase numerical simulations are conducted to analyze the motor flow characteristics exploiting an Eulerian-Eulerian CFD model. The single-phase simulations reveal the presence of circumferential flow and vortices in the nozzle, indicating deviations from an axisymmetrical behavior. However, the impact on motor performance is found to be negligible. Multiphase simulations show the formation of particle-rich regions and relevant azimuthal gradients. This phenomenology provides a reduction of the specific impulse as much as the inflow presents an inhomogeneous distribution of the condensed phase. These findings emphasize the influence of combined 3D and multiphase effects on SRM performance, highlighting the necessity of addressing this topic during the motor design.

1. Introduction

The solid propellant motors (SRM) play a crucial role in the global space transportation system and are utilized by every country with space access. In Europe, these motors are of utmost importance, serving as a vital component in the next-generation vehicles like the Vega and Ariane launchers.

Today, to meet the requirements of an increasingly demanding industry, the most advanced solid motors make use of purely three-dimensional geometries and composite propellant formulations. The most popular configuration chosen by engineers all over the world is represented by the aft-finocyl design: a three-dimensional configuration in which cavities are carved radially in the propellant to give rise to "fins" downstream of a homogeneous 2D zone resembling a hollow cylinder. Upon ignition, the cavities offer a large area over which combustion can take place, but once the fins are depleted, the area exposed (and the consequent thrust) decreases. As a drawback, the evaluation of heat loads, thermal protection erosion, and performance is made much more complex due to the presence of a three-dimensional highly energetic flow. A further resource useful to rise up the specific impulse of this kind of propulsive system involves the loading of aluminum particles into the grain propellant, up to 20% of the total mass. Despite its favorable effect on motor performance, the inclusion of metal particles in the propellant has some side effects. Indeed, it may lead to slag accumulation,[17] thermoacoustic instability,[6] and nozzle mechanical erosion.[21] For the reasons stated above, it is evident that the correct evaluation of such a fully three-dimensional and two-phase flowfield plays a key role in the study of this kind of propulsive system.

As the available scientific literature evinces, taking into account the three-dimensional effects of the SRM internal flow is essential in order to study, analyze, and understand the characteristic phenomena occurring in this class of propulsive systems. In the past years, research groups have employed CFD tools to focus on the flowfield structure generated by complex geometries. Starting from early activities devoted to recovering the flow properties of aft-finocyl design,[5] the actual effects of 3D and two-phase flows have been addressed by authors on a range of different topics: the mechanical and thermochemical nozzle erosion;[18,19] pressure and thrust oscillations,[1] the ignition transient behavior.[15,16] As a matter of fact, all of the cited works highlight how the particular features under analysis are effectively affected by the three-dimensional and multiphase flow.

In this context, the primary objective of this paper is to investigate the behavior of 3D and multiphase flow, which is typical in complex solid rocket motors, focusing specifically on the subject of motor performance, a topic that is often poorly addressed in the existing literature. To accomplish this task, extensive numerical simulations have been conducted on a specially constructed test case during the course of this study.

DOI: 10.13009/EUCASS2023-978

2. CFD Model

The solid rocket motor flowfield is evaluated by solving the compressible and inviscid equations valid for multiphase and non-reacting flows. The governing equations for the gaseous and condensed phases are respectively reported in Eqs.1 and 2:

$$\frac{\partial(\rho_g)}{\partial t} + \nabla \cdot (\rho_g \mathbf{u}_g) = 0 \tag{1a}$$

$$\frac{\partial(\rho_g \mathbf{u}_g)}{\partial t} + \nabla \cdot (\rho_g \mathbf{u}_g \mathbf{u}_g + p) = -\mathbf{F}_d \tag{1b}$$

$$\frac{\partial(\rho E_g)}{\partial t} + \nabla \cdot [(\rho_g E_g + p)\mathbf{u}_g] = -\mathbf{F}_d \cdot \mathbf{u}_p - Q_c \tag{1c}$$

$$\frac{\partial(\rho_p)}{\partial t} + \nabla \cdot (\rho_p \mathbf{u}_p) = 0 \tag{2a}$$

$$\frac{\partial(\rho_p \mathbf{u}_p)}{\partial t} + \nabla \cdot (\rho_p \mathbf{u}_p \mathbf{u}_p) = \mathbf{F}_d \tag{2b}$$

$$\frac{\partial(\rho_p E_p)}{\partial t} + \nabla \cdot (\rho_p E_p \mathbf{u}_p) = \mathbf{F}_d \cdot \mathbf{u}_p + Q_c \tag{2c}$$

where the term $E_g = e_g + \mathbf{u}^2/2$ represents the total energy per unit mass of the gaseous phase, which is the sum of the internal energy $e_g = c_v T$ and the kinetic energy. The same expression holds also for the condensed phase, nevertheless in this case the internal energy is a function of constant specific heat, c_s. Concerning the gaseous set of equations, the caloric equation of state is obtained by expressing the specific heat as a function of the gases temperature according to the seventh-order polynomial:

$$c_p(T) = a_1 T^{-2} + a_2 T^{-1} + a_3 + a_4 T + a_5 T^2 + a_6 T^3 + a_7 T^4 \tag{3}$$

with coefficients $a_{1,i}, a_{2_i}, \ldots, a_{7,i}$ extracted from the Nasa report.[14] The molecular transport properties μ and k are taken from the fourth-order polynomials of temperature.[14]

The employed multiphase model is based on a pressure-less Eulerian approach to describe the dynamics of the alumina particles. The condensed phase is supposed to be dilute and characterized by spherical globules. Finally, a simple monokinetic closure is applied. It is worth noting that such an approach is not suited for large particles due to the impossibility to recover their trajectory crossings, anyway in solid motors, beak-up phenomena reduce the particles size allowing a monokinetic approach to be safely employed.

Several formulas can be used to determine the two-way source terms. In general, they are related to the number of particles per unit of volume, written as:

$$n_p = \frac{6\rho_p}{\pi\, \rho_{Al_2O_3}\, d_p^3} \tag{4}$$

where $\rho_{Al_2O_3}$ represents the alumina density and $d_{p,k}$ the diameter characterizing each group of particles. For what concerns the drag force, the classical law for a cloud of n_p particles, assumed valid for a single group of particles, reads:

$$\mathbf{F}_d = \frac{1}{8}\pi \rho_g d_p^2 n_p C_d\, (\mathbf{u}_g - \mathbf{u}_p)\, |\mathbf{u}_g - \mathbf{u}_p| \tag{5}$$

with the drag coefficient, C_d, evaluated accordingly with the formulation derived by Henderson.[10]

Assuming that radiation is actually negligible,[18] convection is the sole heat exchange phenomenon that is taken into account. Its relation reads:

$$Q_c = \pi \lambda d_p n_p (T_g - T_p) Nu \tag{6}$$

As well as for the drag coefficient, gas rarefaction is taken into account also for the mathematical formulation of the Nusselt number, Nu. In this spirit, the Kavanau and Drake expression is employed.[13]

The flow equations are numerically integrated by an in-house CFD solver largely employed in the solid propulsion framework.[2–4, 7–9] The solver adopts a finite volume Godunov-type formulation with second-order accuracy in space ensured by the van Leer slope-limiter. Convective terms are integrated in time by a second-order Runge-Kutta scheme. The physical domain is discretized using multi-block structured grids.

DOI: 10.13009/EUCASS2023-978

3. Numerical Set-up

The present study focuses on the analysis of a specific test case, which involves a three-dimensional geometry representing a modern upper stage fueled by a solid propellant mixture. The design chosen for the numerical investigation features an aft-finocyl configuration with eleven evenly distributed fins. The gas properties in the simulation are evaluated using the Chemical and Equilibrium Applications code,[14] applied to a typical Al/AP/HTPB propellant with a mean chamber pressure of 80.0 bar. The flame temperature and the burning rate are respectively 3500 K and 9 mm/s, whereas the alumina represents around 30% of the combustion gas mass. Two distinct three-dimensional domains are utilized in this study: one encompasses the entire solid rocket motor, including the combustion chamber and propulsive nozzle, while the other focuses solely on the motor nozzle. To optimize the computational resources, the full 3D domain is substituted with a 1/22 circumferential portion of the motor, taking advantage of the unique design characterized by eleven fins. For the motor simulations, presented in Fig.1, the boundary conditions assume a supersonic outflow, symmetry conditions along the solid wall and lateral faces, and mass flow rate and total temperature over the combustion surface. Additionally, higher mass flow rates are employed to model the gas inflow from the fin cavities into the chamber bore. In particular, the mass flow rate imposed over the connection surface between the fins slots and the cylinder is increased by a factor that takes into account the combustion gases produced within a propellant slot. This approach avoids the need for directly simulating a portion of the combustion chamber, thereby reducing the computational cost for the full motor case. A qualitative sketch is provided in Fig.2 to better illustrate the adopted strategy.

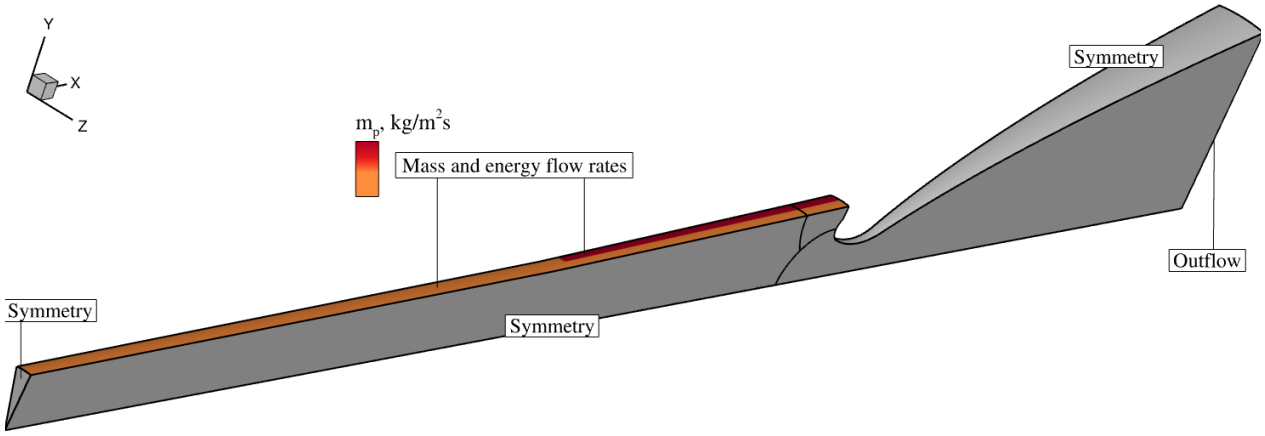

Figure 1: Computational domain and boundary conditions for the case under analysis.

4. Numerical Results

In order to deeply investigate the role of a complex multidimensional domain as that of an aft-finocyl solid rocket motor, both single-phase and multiphase simulations have been performed. In the following sections, results concerning both types of computations are reported.

4.1 Single-phase Simulations

Single-phase computations are employed to investigate the exclusive contribution of a three-dimensional grain configuration on motor performance. In this case, the condensed phase is tackled by means of a heavy-gas approach:[4] the alumina particles are assumed to be homogeneously diluted in the gas, in fluid dynamical and thermodynamical equilibrium with the gaseous mixture. This approach can be seen as a simplification of the two-phase case in which particles are extremely small so that they are able to perfectly follow the gas.

Figure 3 illustrates the steady-state solution of the axial velocity obtained for the SRM case. The flow field associated with the cylindrical portion of the grain exhibits the distinctive structure of Taylor-Culick flow.[20] Notably, near the fin slots, this solution is significantly influenced by the unsymmetric boundary condition, resulting in a discernible azimuthal gradient of the flow property.

Figure.4 provides further insights into the flow by presenting vorticity contours and velocity vectors in a 3D view zoomed over the nozzle region. The shown outcomes highlight the presence of a circumferential flow and vortex generation, indicating a deviation from axisymmetry in the nozzle section. Moreover, the computational results

DOI: 10.13009/EUCASS2023-978

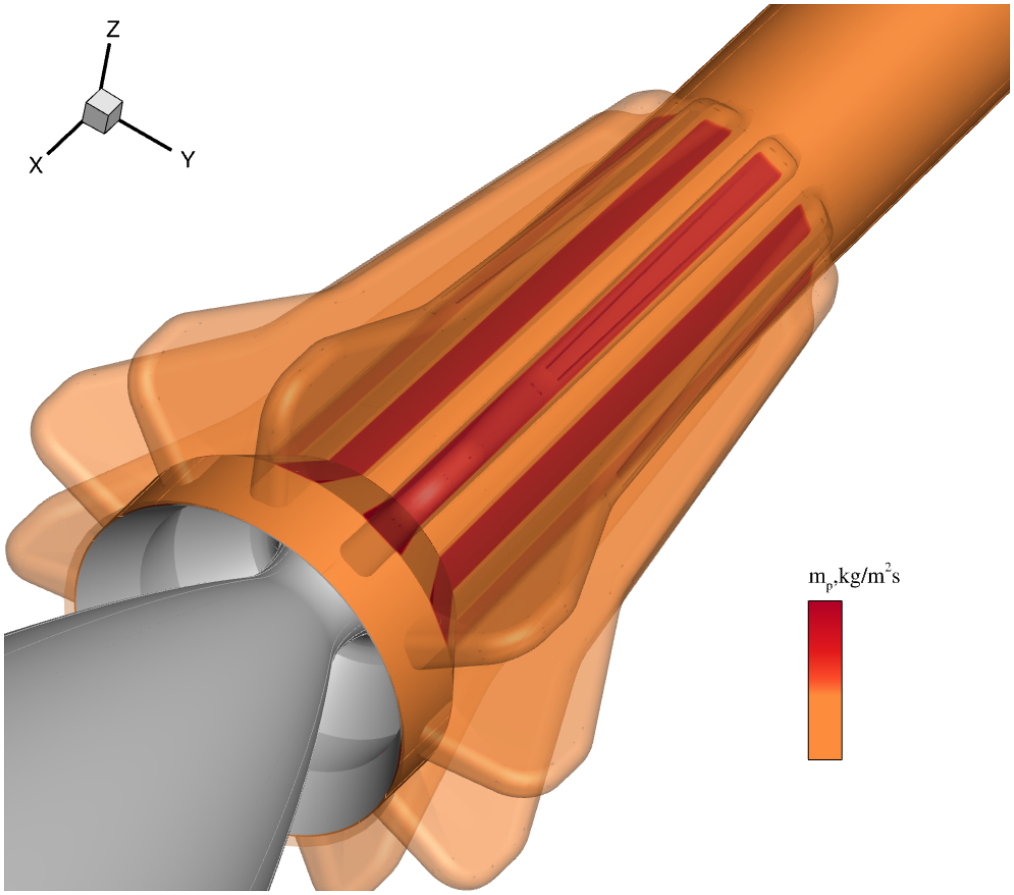

Figure 2: Comparison of boundary conditions for two different set-ups concerning a generic aft-finocyl SRM. In a full simulation, the propellant surface is treated with a uniform combustion velocity (orange), whereas the adopted set-up assumes higher mass and energy rates (red) where the connection between the cylinder and the fins is located.

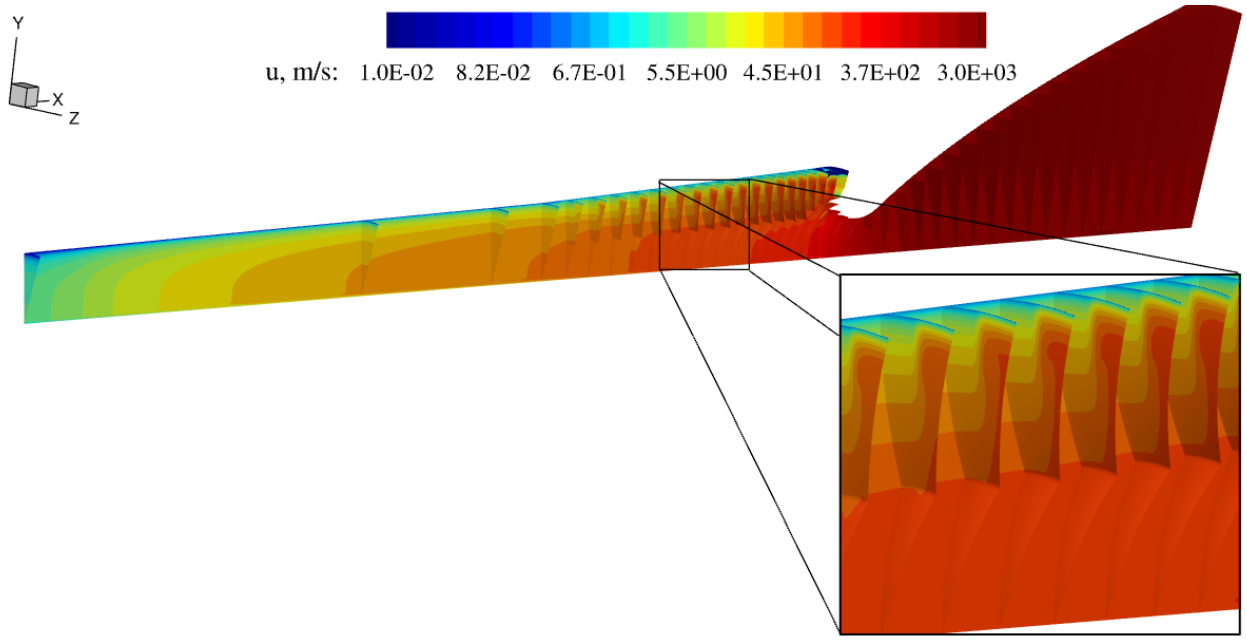

Figure 3: Velocity flow field of the solid rocket motor test case.

DOI: 10.13009/EUCASS2023-978

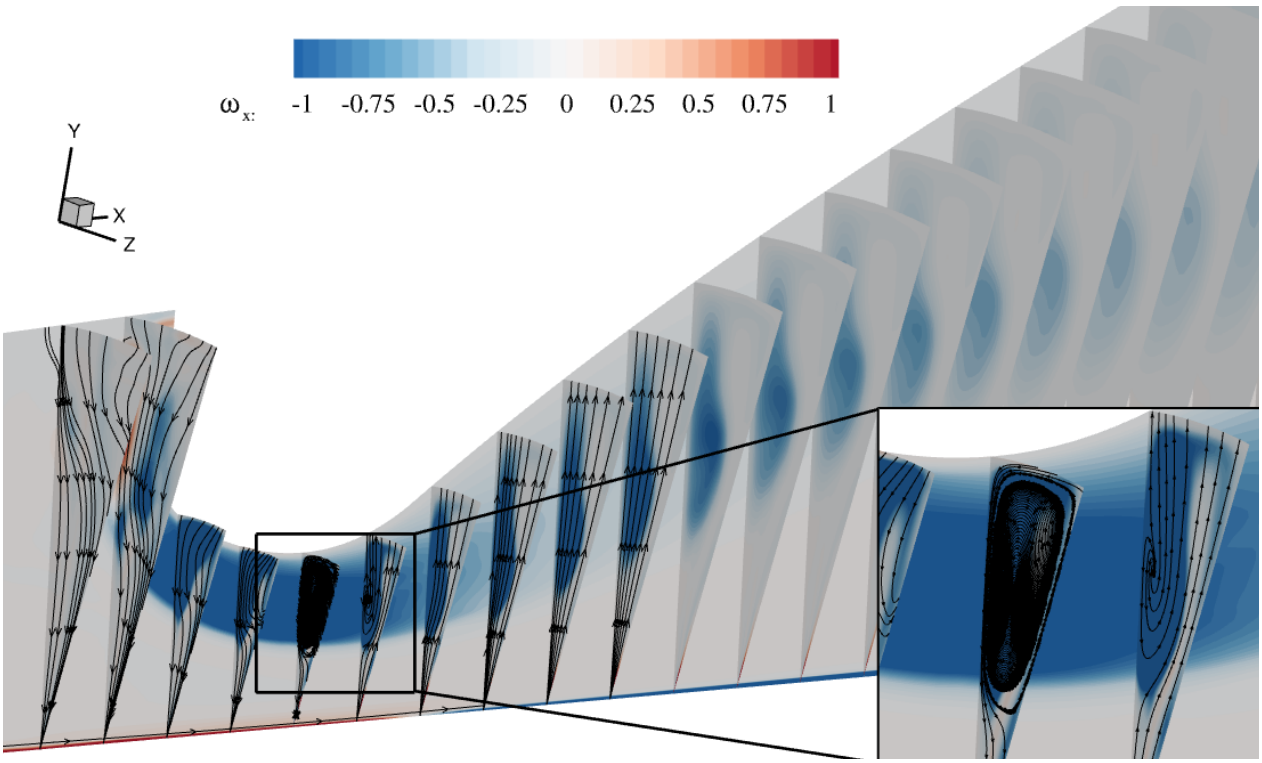

Figure 4: Vorticity flow field and streamlines of the solid rocket motor test case.

demonstrate that the maximum vorticity increases progressively from the chamber bore to the converging part of the nozzle and subsequently decreases within the diverging section. It is noteworthy that the findings described in the present study align with previous observations documented in the scientific literature.[5,12]

The computed internal flow field clearly demonstrates the three-dimensional nature of the flow in the rocket nozzle. However, the role played by this characteristic on motor performance should be assessed. To pursue this aim, a three-dimensional simulation of the motor nozzle is performed assuming a homogeneous inflow in terms of pressure and temperature. To ensure a meaningful comparison, the inflow properties have been defined by averaging the flow quantities extracted over the nozzle inlet surface of the full motor computation. In this spirit, the nozzle mesh is extracted as it is from the motor grid. This analysis aims to compare the same propulsive nozzle working at the same operative point in terms of mass flow rate and pressure but with different distributions of the inflow gases: on one hand, a three-dimensional grain geometry generates and maintains a three-dimensional flow on the nozzle inlet; on the other, the motor design is such to promote uniformity among the combustion gases before entering the converging section of the nozzle. Figure 5 provides a comparison of the velocity flow field for both cases. As it is evident, some differences are actually appreciable, especially within the convergent section, confirming the influence of the grain aft fins on the flow within the nozzle. However, despite the observed distinctions, the effect on motor performance is found to be definitely negligible, as demonstrated by the data presented in Table 1. Specifically, a comparison of the specific impulse calculated for both simulations reveals a close match. This behavior can be reasonably attributed to the tendency of the gases to homogenize just downstream of the throat, providing an almost uniform flow at the nozzle exit.

	SRM	Nozzle
I_{sp}	297.86	297.82

Table 1: Specific impulse evaluated via two different simulation set-ups.

4.2 Multiphase Simulations

In a real scenario, the aluminum oxide particles present in the combustion gases are characterized by mechanical and thermal lag with the gaseous phase. In this work, the contribution of such a phenomenon in a three-dimensional

DOI: 10.13009/EUCASS2023-978

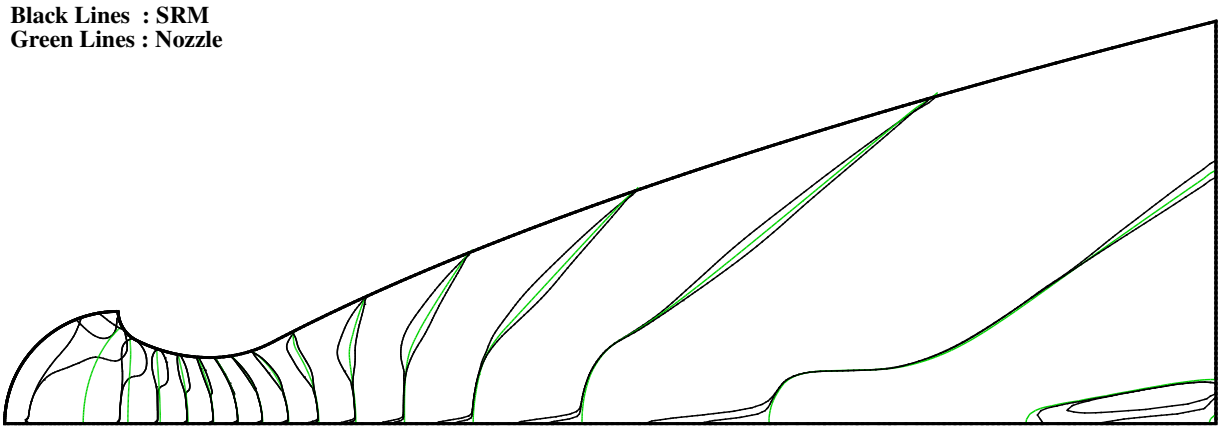

Figure 5: Velocity contour lines for both the lateral faces of the 3D SRM and for the nozzle.

configuration is investigated by means of multiphase simulations concerning only the nozzle domain. This choice is motivated by the inherent limitations of the employed mathematical model. Large alumina globules ($> 100\,\mu m$), produced by the combustion of aluminum agglomerates, may be found within the combustion chamber and upstream of the nozzle throat, where intense shear forces are able to give rise to break-up phenomena which reduce the mean particles size in the divergent section of the nozzle. Nevertheless, the monokinetic Eulerian model used in the present work to study the dynamics of the condensed phase is not suitable for accurately describing the behavior of large particles, hence a multiphase solution of the whole motor can not be taken into account. On the other hand, previous analyses conducted by the authors[8] have shown that the model presented in Sec.2 applied to the sole nozzle yields a reliable estimation of the motor performance. Given these premises, the combined effects of multiphase and multidimensional contributions on the motor specific impulse are investigated by simulating only the nozzle domain, while the inflow properties are parametrized to account for the different distributions of alumina particles at the nozzle inlet. Regarding this matter, two extreme conditions can be considered. The first condition assumes that the particles size, grain geometry, and flow properties are such that the condensed phase has achieved a uniform distribution in front of the converging section of the nozzle. In this case, the alumina particles are evenly dispersed, and there is no significant variation in their azimuthal distribution. On the other hand, the second condition represents the maximum azimuthal non-uniformity. This scenario occurs when the alumina particles produced within the fin slots remain confined to the same angular sector due to their high inertia and flow conditions that prevent their redistribution. As a result, there is a notable lack of azimuthal particle dispersion, leading to a highly non-uniform distribution. By considering these two limit conditions, the study aims to assess the best and the worst cases concerning the influence of the alumina particle distribution on the nozzle performance.

The set-up of the numerical simulations performed within this phase of the study is very similar to the one described in the previous section for the nozzle domain. Details are reported in Fig.6. For what regards the condensed phase, the Hermsen[11] expression for the De Brouckere volume-weighted mean diameter, or d_{43}, is assumed to define the particles size which, for the specific case under analysis, is worth approximately 7 μm. The inflow area is split into two separate surfaces to take into account different particles mass flux depending on the azimuthal sector. Figure 6b collects the mass flow rates used in the parametric input depending on the non-uniformity level. The 0% and 100% represent the two limit conditions described above. The alumina droplets are injected into mechanical and thermal equilibrium with the gas. Finally, in the spirit of focusing solely on the performance viewpoint, the gaseous phase is homogeneously injected over the whole inflow surface.

The numerical results valid for the 50% non-uniformity level are presented in Fig.7. As it is evident in the particles density flowfield of Fig.7a, the non-uniformity of the inflow of particles is maintained throughout the entire domain, leading to an azimuthal density gradient of the condensed phase. Furthermore, the particles non-uniformity significantly disrupts the axisymmetric structure of the gas flow, as illustrated in the velocity field depicted in Fig.7b. Indeed, in angular sectors characterized by higher particle density, the gas flow experiences a notable decrease in velocity due to the increased amount of particles which slow down the gas flow.

Figure 8 provides an overview of the particle density and gas velocity distribution in the multiphase flow field. Both flow properties, extracted from the nozzle exit section at the middle height, are plotted as functions of the azimuthal angle. The numerical results show that by increasing the non-uniformity of the particles inflow, the azimuthal gradient

DOI: 10.13009/EUCASS2023-978

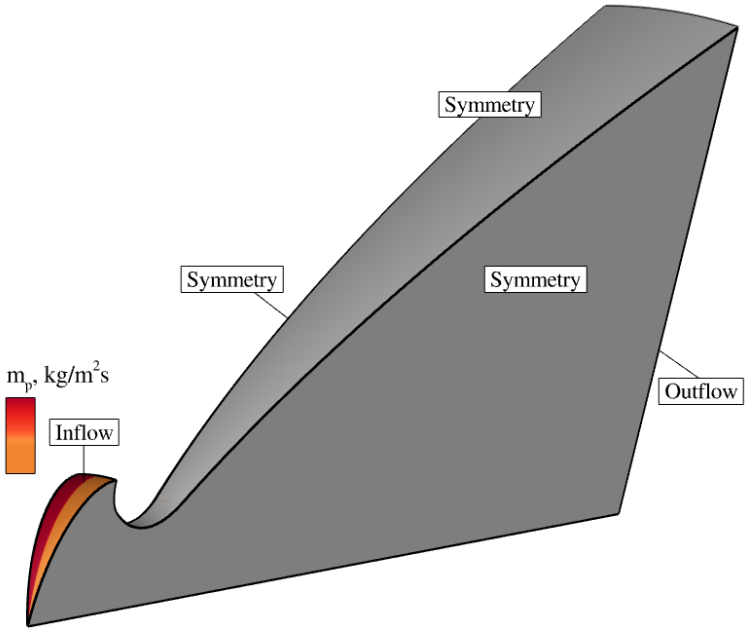

(a) Three-dimensional domain with boundary conditions.

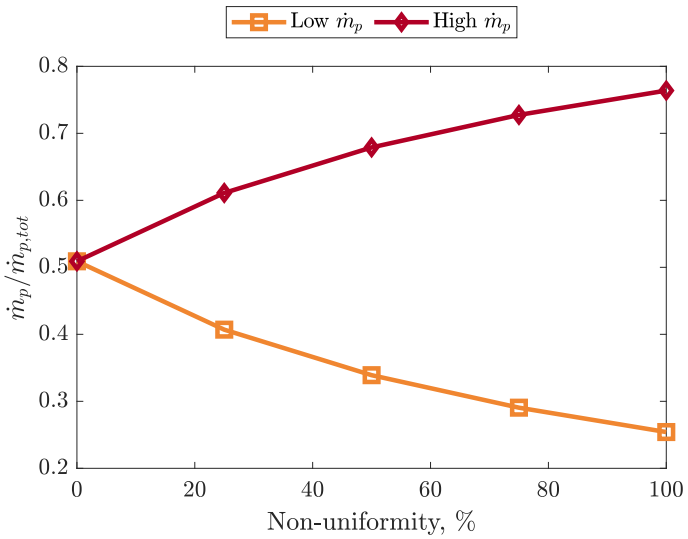

(b) Parametric input of the particles mass flow rate. Values are normalized with regard to the overall particles mass flux.

Figure 6: Computational domain and parametric boundary conditions for multiphase simulations.

of the flow characteristics tends to grow up providing a solution increasingly distant from the homogeneous distribution shown by the 0% case. Note that this case should present a perfectly uniform trend, although, very slight deformations may be observed due to the effect of the lateral boundaries of the domain. Additionally, an interesting observation is the widening of the particle-rich region as the condensed phase is injected in a non-uniform manner. This phenomenon can be attributed to a memory effect originating from upstream conditions. In the convergent section of the nozzle, the initially split distribution around $\theta = 0°$ is disrupted as the converging flow enables particles injected through the high mass flux region to pass through the symmetry plane. This configuration is subsequently maintained in the divergent section due to the inertia of the condensed phase and the dynamics of the flow.

The effect of the described phenomenology on the performance viewpoint is pictured in Fig.9. As it is possible to observe, the specific impulse undertakes a monotonic and almost linear reduction as the non-uniformity level of the particles inflow grows. In particular, the worst case exhibits a 0.5% diminution which means more than 1 second in this specific case. It is worth noting that this result, in terms of quantitative outcomes, is strictly limited to the analyzed

DOI: 10.13009/EUCASS2023-978

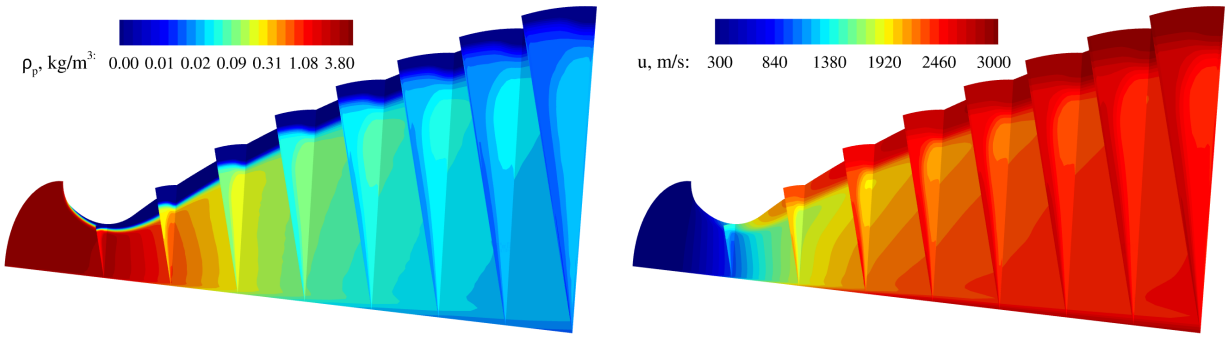

(a) Particles density. (b) Gas velocity.

Figure 7: Computed flowfields for the 50% level of non-uniformity.

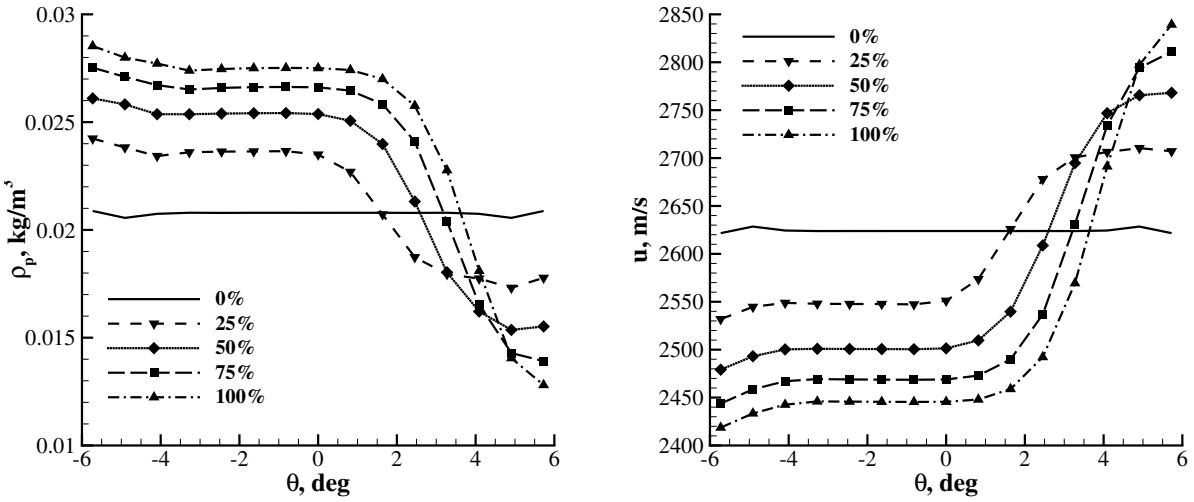

(a) Particles density. (b) Gas velocity.

Figure 8: Comparison of the flow properties when varying the non-uniformity level of the particles inflow.

test case, on the other hand, the observed trend may be assumed as fully general and represent an interesting effect of multiphase and multidimensional flows in solid rocket motors.

5. Conclusions

In conclusion, this study focused on the analysis of multiphase and multidimensional contributions to the performance of modern solid rocket motors. To achieve this task, numerical simulations were conducted on a specific test case involving a three-dimensional aft-finocyl geometry of a modern upper stage fueled by a solid propellant mixture.

Single-phase simulations were first performed to examine the exclusive contribution of the three-dimensional grain configuration to the motor performance. The results showed the presence of a circumferential flow and vortex generation, indicating a deviation from axisymmetry in the nozzle section. However, despite the observed differences in the flow field, the effect on motor performance, as quantified by the specific impulse, was found to be negligible. The gases tend to homogenize downstream of the throat, providing an almost uniform flow at the nozzle exit.

Multiphase simulations were then conducted to investigate the combined effects of multiphase and multidimensional contributions on the motor performance. These simulations focused on the nozzle domain and considered the distribution of alumina particles in the combustion gases. Two extreme conditions were considered: a uniform distribution of particles and a highly non-uniform distribution. The results showed that the non-uniformity of the particle distribution disrupted the axisymmetric structure of the gas flow and led to an azimuthal density gradient of the condensed phase. The particle-rich region widened with increasing non-uniformity, indicating a memory effect originating from upstream conditions.

DOI: 10.13009/EUCASS2023-978

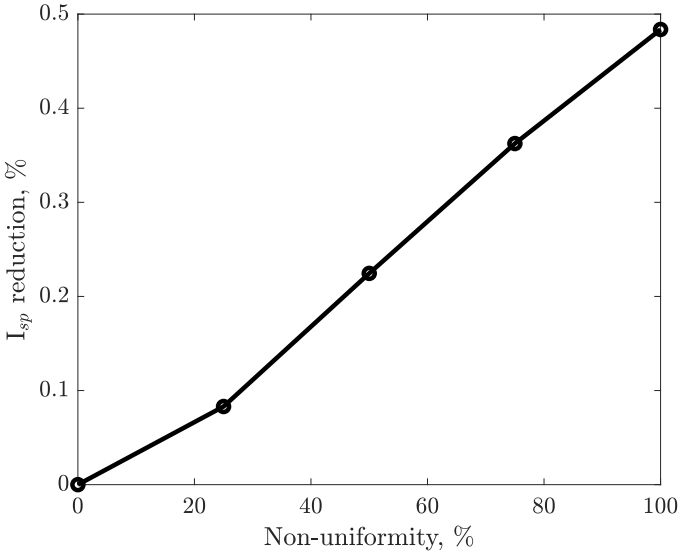

Figure 9: Specific impulse trend at varying inflow non-uniformity.

Overall, the findings of this study highlighted the three-dimensional nature of the flow in the rocket nozzle and the influence of the grain aft fins on the flow. The effect on motor performance, as evaluated by the specific impulse, was found to monotonically reduce with the level of non-uniformity of the condensed phase, with a relative reduction of 0.5% for the specific case under analysis. These outcomes contribute to a better understanding of the flow behavior in complex solid rocket motors and provide insights for the design and optimization of such propulsion systems.

Further investigations could focus on refining the modeling and simulation approaches to better capture the behavior of large alumina particles within the combustion chamber, an operation that would allow us to compute in a more rigorous and tangible manner the nozzle inflow conditions.

References

[1] S. Ballereau, F. Godfroy, O. Orlandi, and D. Ballion. Numerical simulations and searching methods of thrust oscillations for solid rocket boosters. In *AIAA/ASME/SAE/ASEE 42nd Joint Propulsion Conference*, pages 1059–1073, 2006.

[2] Daniele Bianchi and Francesco Nasuti. Navier-stokes simulation of graphite nozzle erosion at different pressure conditions. *AIAA Journal*, 53(2):356–366, 2015.

[3] Daniele Bianchi, Francesco Nasuti, and Marcello Onofri. Radius of curvature effects on throat thermochemical erosion in solid rocket motors. *Journal of Spacecraft and Rockets*, 52(2):320–330, 2015.

[4] Daniele Bianchi and Agostino Neri. Numerical simulation of chemical erosion in vega solid-rocket-motor nozzles. *Journal of Propulsion and Power*, 34(2):482–498, 2018.

[5] Bruno Chaouat. Flow analysis of a solid propellant rocket motor with aft fins. *Journal of Propulsion and Power*, 13(2):194–196, 1997.

[6] S. Gallier and F. Godfroy. Aluminum combustion driven instabilities in solid rocket motors. *Journal of propulsion and power*, 25(2):509–521, 2009.

[7] Marco Grossi, Daniele Bianchi, and Bernardo Favini. Modeling multiphase effects on pressure oscillations in solid propulsion. In *AIAA Propulsion and Energy 2020 Forum*, page 3927, 2020. AIAA Paper 2020-3927.

[8] Marco Grossi, Alessio Sereno, Daniele Bianchi, and Bernardo Favini. Multiphase effects on solid rocket nozzle performance. *Journal of Propulsion and Power*, 2023.

[9] Marco Grossi, Alessio Sereno, Daniele Bianchi, and Bernardo Favini. Role of finite-rate kinetics on the performance predictions of solid rocket motor nozzles. In *AIAA SciTech 2023 Forum*, page 1314, 2023.

DOI: 10.13009/EUCASS2023-978

[10] Charles B Henderson. Drag coefficients of spheres in continuum and rarefied flows. *AIAA Journal*, 14(6):707–708, 1976.

[11] RW Hermsen. Aluminum oxide particle size for solid rocket motor performance prediction. *Journal of Spacecraft and Rockets*, 18(6):483–490, 1981.

[12] W JOHNSTON. A computational fluid dynamics analysis of the internal flow in a titan srmu. In *26th Joint Propulsion Conference*, page 2079, 1990.

[13] Lawrence Lewis Kavanau and RM Drake Jr. Heat transfer from spheres to a rarefied gas in subsonic flow. Technical report, California University of Berkley, Institute of Engineering Research, 1953.

[14] B. J. McBride and S. Gordon. Computer program for calculation of complex chemical equilibrium compositions and applications. NASA RP-1311, National Aeronautics and Space Administration, 1994.

[15] Jeffrey D Moore, Kenneth K Kuo, and Peter J Ferrara. Flame-spreading behavior in a fin-slot solid propellant rocket motor grain (part ii). *Journal of Propulsion and Power*, 25(3):808–814, 2009.

[16] Jeffrey D Moore, Robert B Wehrman, Kenneth K Kuo, Peter J Ferrara, and Ryan W Houim. Flowfield structure in a fin-slot solid rocket motor (part i). *Journal of Propulsion and Power*, 25(2):499–508, 2009.

[17] Mark Salita. Deficiencies and requirements in modeling of slag generation in solid rocket motors. *Journal of Propulsion and Power*, 11(1):10–23, 1995.

[18] Toru Shimada, Yu Daimon, and Nobuhiro Sekino. Computational fluid dynamics of multiphase flows in solid rocket motors. Technical report, Japan Aerospace Exploration Agency (JAXA), 2006.

[19] Toru Shimada, Masumi Sekiguchi, and Nobuhiro Sekino. Flow inside a solid rocket motor with relation to nozzle inlet ablation. *AIAA journal*, 45(6):1324–1332, 2007.

[20] Geoffrey Ingram Taylor. Fluid flow in regions bounded by porous surfaces. *Proceedings of the Royal Society of London. Series A. Mathematical and Physical Sciences*, 234(1199):456–475, 1956.

[21] Piyush Thakre, Rajesh Rawat, Richard Clayton, and Vigor Yang. Mechanical erosion of graphite nozzle in solid-propellant rocket motor. *Journal of Propulsion and Power*, 29(3):593–601, 2013.